Conformationally Mobile Acyclic Cucurbit[n]uril-Type Receptors Derived from an S-shaped Methylene Bridged Glycoluril Pentamer

Kimberly G. Brady,[†] Laura Gilberg,[†‡] David Sigwalt,[†] Joshua Bistany-Riebman,[†] Steven Murkli, [†] Jared Klemm,[†] Petr Kulhánek,[$] Vladimír Šindelář,*[‡] and Lyle Isaacs*[†]*

[†] Department of Chemistry and Biochemistry, University of Maryland, College Park, Maryland 20742, United States; [$] CEITEC - Central European Institute of Technology and [‡] Department of Chemistry and RECETOX, Faculty of Science, Masaryk University, Kamenice 5, 625 00 Brno, Czech Republic

*To whom correspondence should be addressed. Prof. Lyle Isaacs, Email: LIsaacs@umd.edu; Dr. Petr Kulhánek, Email: kulhanek@chemi.muni.cz; Prof. Vladimír Šindelář, Email: sindelar@chemi.muni.cz

Abstract: We report the synthesis of the conformationally mobile S-shaped glycoluril pentamer building block **3a** and two new acyclic CB[n]-type receptors **P1** and **P2**. **P1** (9 mM) and **P2** (11 mM) have moderate aqueous solubility but their host•guest complexes are poorly soluble. Host **P1** does not undergo intermolecular self-association whereas **P2** does (K_s = 189±27 M^{-1}). ^{1}H NMR titrations show that **P1** and **P2** are poor hosts toward hydrophobic (di)cations **6** – **11** (**P1**: K_a = 375–1400 M^{-1}; **P2**: K_a = 1950–19800 M^{-1}) compared to **Tet1** and **Tet2** (**Tet1**: K_a = 3.09 x 10^6 to 4.69 x 10^8 M^{-1}; **Tet2**: K_a = 4.59 x 10^8 to 1.30 x 10^{10} M^{-1}). Molecular modelling shows that **P1** and **P2** exist as a mixture of three different conformers due to the two S-shaped methylene bridged glycoluril dimer subunits that each possess two different conformations. The lowest energy conformers of **P1** and **P2** do not feature a well-defined central cavity. In the presence of guests, **P2** adapts its conformation to form 1:1 **P2**•guest complexes; the binding free energy pays the energetic price of conformer selection. This energetically unfavorable conformer selection results in significantly decreased K_a values of **P1** and **P2** compared to **Tet1** and **Tet2**.

Keywords: acyclic cucurbituril, molecular recognition, isothermal titration calorimetry, foldamer

Introduction. Over the past two decades, there have been great advances in the preparation of members of the cucurbit[n]uril (n = 5, 6, 7, 8, 10, 13-15, Figure 1) family of molecular container compounds.[1] The defining features of CB[n] molecular containers are their two symmetry equivalent ureidyl carbonyl portals which are highly electrostatically negative and their central hydrophobic cavity.[2,3] Given these structural features, CB[n] are excellent hosts for hydrophobic (di)ammonium ions which often bind with K_a values in the $10^6 - 10^9$ M^{-1} range and in select cases with K_a values exceeding 10^{12} M^{-1} in aqueous solution.[3,4] The high affinity of macrocyclic CB[n]•guest complexes has been traced to the presence of high energy waters in the cavity of CB[n] that are released upon complexation.[5] CB[n] hosts are also quite selective and large differences in K_a values are seen upon application of suitable stimuli (e.g. pH, electrochemical, photochemical).[6,7] Accordingly, CB[n] have emerged as an outstanding platform for the development of functional supramolecular systems including chemical sensors, molecular machines, supramolecular polymers and materials, and drug delivery systems.[7,8] In recent years, the development of methods to prepare per- and mono-functionalized CB[n] hosts have allowed their strategic merger with polymers, solid phases, surfaces, nanoparticles, targeting ligands, antibodies, and fluorophores which has further extended their applicability in the chemical, biological, and biomedical arenas.[9]

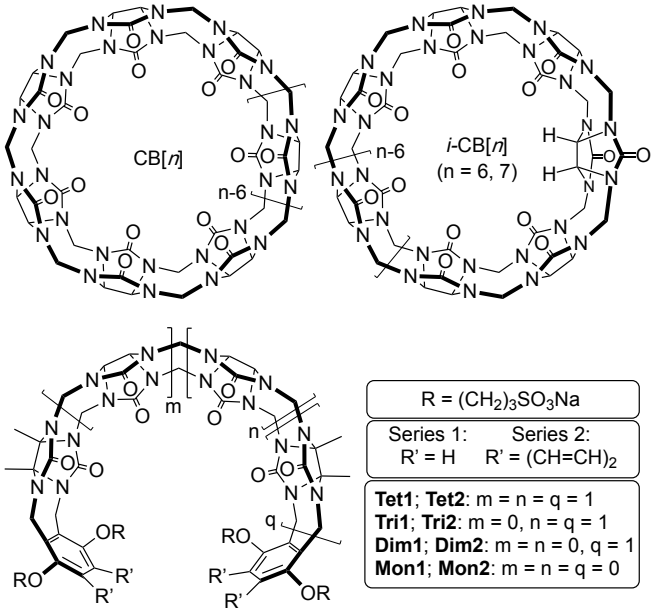

Figure 1. Chemical structures of CB[*n*], *i*-CB[*n*] with one inverted glycoluril unit, and acyclic CB[*n*]-type receptors.

Over the years, the Isaacs and Šindelář groups have been very interested in the mechanism of CB[n] formation, especially the formation of the S-shaped and C-shaped diastereomeric methylene bridged glycoluril dimers.[10,11-13] The S-shaped forms are kinetic products whereas the C-shaped forms are the thermodynamic products which eventually lead to macrocyclic CB[n] by cyclooligomerization.[14] Inverted CB[n] (*i*-CB[n], Figure 1) have also been isolated;[15] *i*-CB[n] feature a pair of methine H-atoms pointing into the CB[n] cavity and possess a pair of adjacent S-shaped units. The binding affinity of *i*-CB[n] (n = 6, 7) toward typical hydrophobic ammonium ions are weaker than the corresponding diastereomeric CB[n].[15] More recently, we have described the preparation of a class of receptors that feature a central glycoluril oligomer that is capped with two terminal aromatic walls (e.g. **Tet1** and **Tet2**, Figure 1).[16,17] By virtue of their glycoluril oligomer backbone, these receptors are preorganized into a C-shape and retain the essential binding features of the CB[n] family (e.g. tight and selective recognition of hydrophobic

(di)cations). Accordingly, these hosts are referred to as acyclic CB[n]-type receptors. Numerous variants have been created, by us and others, that differ in the nature of the central glycoluril oligomer, the terminal aromatic walls, and the appended solubilizing groups.[16,18] Of the acyclic CB[n] based on glycoluril tetramer prepared to date, **Tet1** and **Tet2** have been used extensively because of their high binding affinity which has enabled their function as solubilizing excipients for insoluble drugs and as *in vivo* sequestration agents for neuromuscular blockers (e.g. rocuronium and vecuronium)[19,20] and drugs of abuse such as methamphetamine.[21] Host **Tet1** has displayed excellent biocompatibility according to the usual *in vitro* (e.g. cell death and metabolic activity, mutagenicity, lack of hERG ion channel inhibition) and *in vivo* (e.g. maximum tolerated dose, blood gases, blood pH, mean arterial pressure) assays.[16] The group of Prof. Ruibing Wang has used macrocyclic CB[7] as a sequestering agent in related applications.[22] Previously, we have prepared and studied the molecular recognition properties of analogues of **Tet1** and **Tet2** based on central glycoluril monomer, dimer, and trimer (**Mon1** – **Tri1** and **Mon2** – **Tri2**).[23] We found that **Mon1** – **Tri1** and **Mon2** – **Tri2** do not function well as solubilizing agents for insoluble drugs due to their smaller cavities which result in lower binding constants. Accordingly, we wondered whether acyclic CB[n]-type receptors that feature an extended glycoluril oligomer (e.g. pentamer) might display higher binding affinity toward their guests than **Tet1** and **Tet2** and therefore function as superior sequestration agents. In this paper, we describe the synthesis of pentamer derived acyclic CB[n] hosts **P1** and **P2** and investigations of their molecular recognition properties.

Results and Discussion. This results and discussion section is organized as follows. First, we describe the design, synthesis, and characterization of hosts **P1** and **P2**. Second, we measure the solubility of **P1** and **P2** in water. Third, we performed ^{1}H NMR titrations to determine the K_a

values of **P1** and **P2** toward guests **6** – **11**. Finally, we discuss the trends in K_a values of **P1** and **P2** toward their guests using **Tet1** and **Tet2** as comparators and rationalize the observed changes based on molecular modelling studies.

Goal of the Study. The initial goal of this study was to determine the impact of the extension of the glycoluril oligomer backbone from tetramer (e.g. **Tet1** and **Tet2**) to pentamer on the molecular recognition properties toward typical cationic guests. In the process, however, we uncovered that the synthesized pentamer hosts **P1** and **P2** feature two S-shaped units that endow them with conformational flexibility. Accordingly, we expanded our study to include the influence of conformational isomerism on guest binding.

Synthesis and Characterization of Pentamer Bis(Cyclic Ether) 3a and Hosts P1 and P2. To prepare acyclic CB[n]-type hosts derived from glycoluril pentamer, we took advantage of a building block approach that relies on the double electrophilic aromatic substitution reaction between a central glycoluril oligomer and a dialkoxy aromatic wall. The condensation of glycoluril (**1**) with dimethylglycoluril bis(cyclic ether) (**2**) which was conducted at lower temperature (90% aq. $MeSO_3H$, 8-12 ˚C) in order to control the oligomerization process gave a complex crude reaction mixture from which we could isolate a single methylene bridged glycoluril pentamer (**3**) in gram scale batches (Scheme 1). The ES-MS spectrum of **3** confirms its molecular formula ($C_{38}H_{46}N_{20}O_{12}$) and that it is composed of two equivalents of **1** and three equivalents of **2**. Because the substituents on the convex face of adjacent glycoluril rings may point in the same or opposite directions (e.g. C-shaped or S-shaped units), there are 10 possible diastereomers of **3**. The four diastereomers (**3a** – **3d**) depicted in Scheme 1 are C_{2v}-symmetric whereas the six

diastereomers that are not shown are C_s-symmetric. The ^{1}H NMR spectrum of **3** recorded in DMSO-d_6 shows three distinct resonances for the methyl groups ($H_k - H_m$), three pairs of doublets for the diastereotopic methylene bridges ($H_c - H_h$), and a pair of doublets for the glycoluril methines (H_i and H_j). Similarly, the ^{13}C NMR spectrum of **3** in DMSO-d_6 displays a total of 14 resonances which is only consistent with a C_{2v}-symmetric structure. Compound **3c** corresponds to the desired glycoluril pentamer that consists of all C-shaped subunits. In contrast, **3a** and **3b** contain 2 S-shaped and 2 C-shaped segments whereas **3d** possesses 4 S-shaped segments. Given the known thermodynamic preference for the C-shaped diastereomers,[10,13] we initially presumed that we had isolated **3c** and subsequently proceeded to create the pentamer derived hosts. It was only later, after observing the poor molecular recognition properties of **P1** and **P2** that we discovered that in reality we had isolated **3a**. The relative stereochemistry of **3a**, **P1**, and **P2** were fully assigned by a combination of ^{1}H, ^{13}C, selective 1D NOE, and 2D NMR experiments (Supporting Information). In brief, once the ^{1}H NMR has been fully assigned, we can use the selective 1D NOE experiments to step from the cyclic ether termini of **3a** toward the center determining relative stereochemistry at each step along the way. As shown in Figure 2, H_c, H_d, and $(CH_3)_l$ show NOEs when $(CH_3)_k$ is irradiated. The resonance for $(CH_3)_l$ shows NOEs to H_e, H_f, and most importantly H_i which establishes the C-shaped relative stereochemistry of the terminal pairs of glycolurils. Proton H_i is coupled to and shows an NOE to the adjacent H_j. Irradiation of H_j shows a main NOE to H_j and very small NOEs to H_g and H_h but does not show an NOE to $(CH_3)_m$ which establishes that the central glycoluril is connected to its neighbors by S-shaped stereochemistry. The identity of H_g and H_h as adjacent to the central glycoluril was confirmed by HMBC cross peaks from H_g and H_h to the central O=C_y which is a half-intensity resonance. From our previous studies of methylene bridged glycoluril dimers we know that the

CH_2-bridges involved in S-shaped connections have smaller $^3J_{HCH}$ coupling constants that those involved in C-shaped connections (≈13.6 Hz vs. ≈16.0 Hz).[10,11,13] The observed coupling constant between H_g and H_h ($^3J_{HCH}$ = 13.7 Hz) of **3a** further supports the depicted diastereomer.

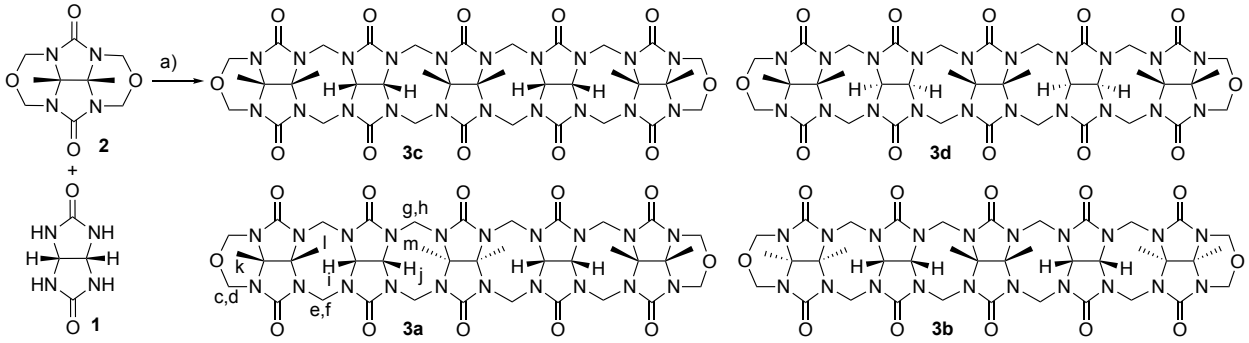

Scheme 1. Synthesis of methylene bridged glycoluril pentamer **3a**. Compounds **3b** – **3d** were not isolated. Conditions: a) 90% aq. $MeSO_3H$, 8-12 ˚C (2 h) then RT (2 h), 5%.

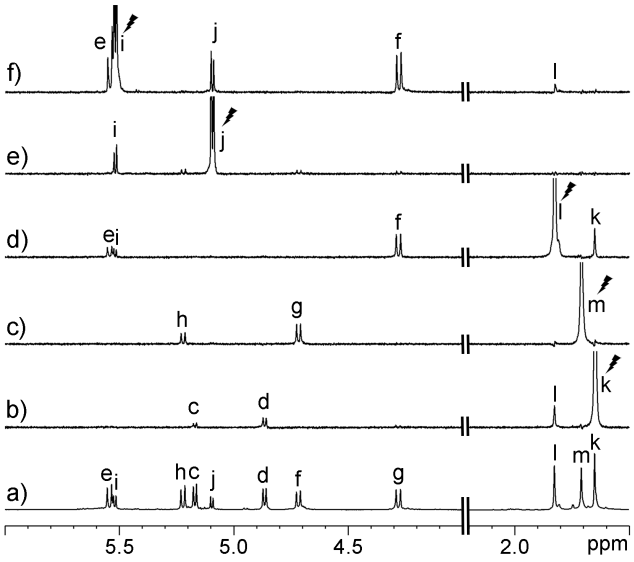

Figure 2. NMR spectra recorded (800 MHz, 30 °C, DMSO-d_6) for **3a**: a) ^{1}H NMR spectrum. Selective 1D NOE recorded for **3a** with irradiation of: b) H_k, c) H_m, d) H_l, e) H_j, and f) H_i.

The sulfonated dialkoxy benzene and dialkoxy naphthalene sidewalls (**4** and **5**) required to synthesize hosts **P1** and **P2** were available from previous studies.[24] As shown in Scheme 2, the attachment of walls **4** and **5** to pentamer **3a** was conducted under acidic conditions (TFA, 75 ˚C) in the presence of Ac_2O to increase reactivity[25] to deliver **P1** (22%) and **P2** (27%) after purification by trituration with hot water (**P1**) and by precipitation from water (**P2**). Hosts **P1** and **P2** were characterized by spectroscopic means. The high resolution electrospray ionization mass spectra for **P1** displayed an ion at *m/z* 547.8031 ($[M-4Na+H]^{3-}$, calculated for $C_{62}H_{75}N_{20}O_{26}S_4$ 547.8020) whereas **P2** displayed an ion at *m/z* 872.2222 ($[M-4Na+2H]^{2-}$, calculated for $C_{70}H_{80}N_{20}O_{26}S_4$ 872.2223) which establish the molecular formulas required of **P1** and **P2**. Figure 3 shows the ^1H NMR spectra recorded for **P1** and **P2** in DMSO-d_6. As expected, host **P1** exhibits a singlet for the four symmetry equivalent H_a protons, three resonances for the methyl groups (H_k, H_l, H_m), a pair of doublets for the equatorial methine protons (H_i and H_j), three pairs of doublets for the bridging methylene groups (H_c – H_h) in the required 4:4:4:4:4:4 ratio, and three resonances for the $O(CH_2)_3SO_3Na$ sidearms expected for a C_{2v}-symmetric structure (Figure 3a). Figure 3b shows the fully assigned ^1H NMR spectrum for **P2** which displays a similar pattern of resonances in accord with C_{2v}-symmetry. The ^{13}C NMR spectra recorded for **P1** (**P2**) display 20 (22) resonances (Supporting Information, Figures S10 and S21) in accord with the 20 (22) resonances expected based on C_{2v}-symmetry. As described above for **3a**, the relative stereochemistry of the glycoluril units of **P1** and **P2** was established based on the combined inference of ^1H, ^{13}C, COSY, HSQC, HMBC, and NOE experiments (Supporting Information). After having firmly established the constitutions and relative stereochemistry of **P1** and **P2** we moved on to determine their inherent solubility in aqueous solution. For this purpose, samples of **P1** and **P2** were weighed on a microbalance and then dissolved in at room temperature in the smallest amount of D_2O possible

with the aid of sonication; the obtained solubility of **P1** (≈ 9 mM) and **P2** (≈ 11 mM) was then calculated in the standard way using the known mass, molecular weight, and volume.

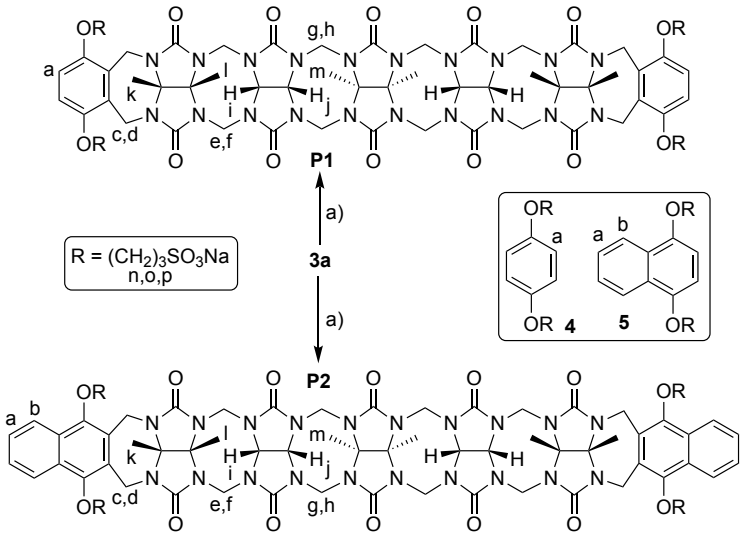

Scheme 2. Synthesis of acyclic CB[*n*]-type receptors **P1** and **P2**. Conditions: a) **4** or **5**, Ac_2O, TFA, 75 °C, **P1**: 22%; **P2**: 27%.

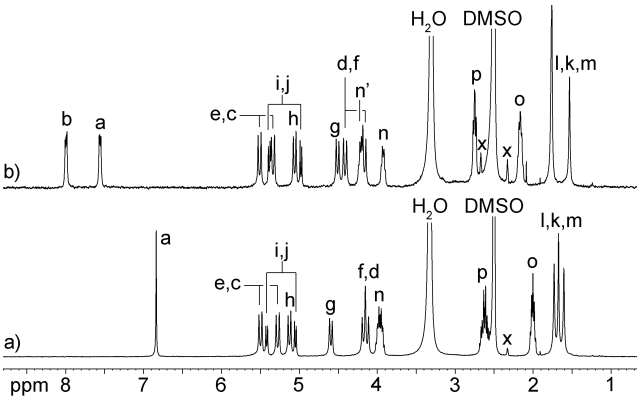

Figure 3. ^{1}H NMR spectra recorded (400 MHz, DMSO-d_6, RT) for: a) **P1**, and b) **P2**. x = ^{13}C satellite.

Conformational Properties of Pentamer Derived Hosts P1 and P2. The chemical structures of **3a** and hosts **P1** and **P2** contain two S-shaped connections between adjacent glycolurils (e.g. the substituents at the equator of the glycoluril units are on opposite sides of the oligomer chain). From previous work, we know that each S-shaped segment can adopt two different conformations where the substituents on the convex face of one glycoluril point toward the concavity of the other glycoluril and vice versa.[10,11,13] Accordingly, there are three distinct conformations for compounds **3a**, **P1**, and **P2**; Figure 4 depicts the three conformers (folds) of **P1** which we refer to as **P1**-F1, **P1**-F2, and **P1**-F3. From previous work, we also know that symmetrical S-shaped methylene bridged glycoluril dimers bearing H-atoms[13] or CO_2Et groups[10,11] on their convex face undergo fast conformational exchange processes between the two chemically equivalent and isoenergetic S-shaped conformations such that the H-atoms on the bridging CH_2-groups are rendered chemically equivalent and appear as a singlet in the ^{1}H NMR spectrum. Finally, the sharp ^{1}H NMR spectra observed (Figure 3) for **P1** and **P2** display the number of resonances expected for C_{2v}-symmetric **P1**-F1 or **P1**-F3 but not for C_s-symmetric **P1**-F2. This result indicates that **P1** (**P2**) is either fixed in the **P1**-F1 or **P1**-F3 (**P2**-F1 or **P2**-F3) folded form or is undergoing fast conversion between all three conformers on the chemical shift timescale. Experimentally, no significant changes in the ^{1}H NMR of **P2** were observed upon cooling to 10 ˚C in D_2O. It should be noted that **P1**-F1 features two terminal molecular clip-like clefts[26] shaped by one aromatic wall, whereas **P1**-F3 possesses a potential cavity that is reminiscent of *i*-CB[n]. The flexibility of sidearms in **P1**-F3 does not forbid induced cavity formation upon guest binding.

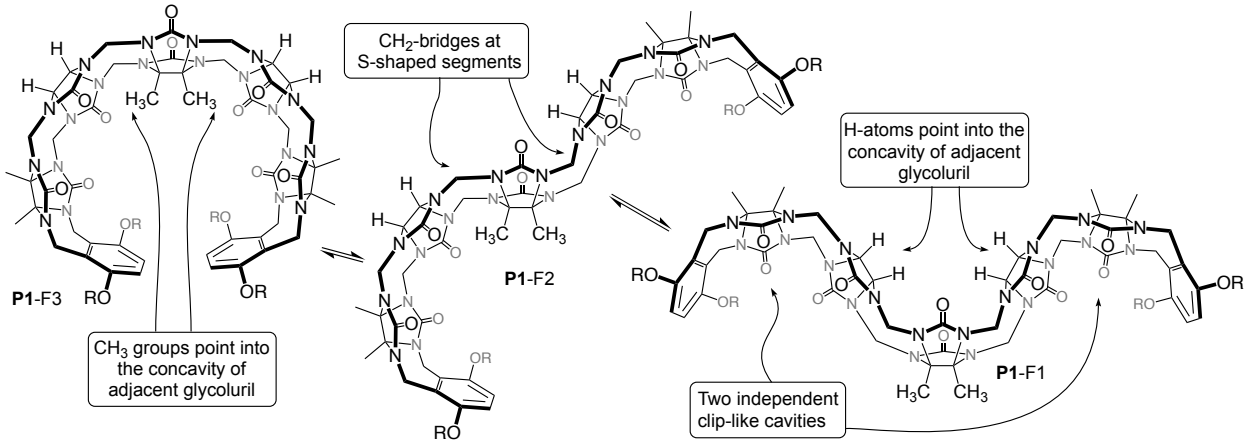

Figure 4. Representations of the different conformational isomers of **P1** that occur by flipping at the S-shaped methylene bridges.

To gain insights into the relative populations of the different conformational states, computational methods using DFT were employed. To decipher the structural features of the methylene bridged glycoluril pentamer containing an inverted glycoluril unit, model systems comprising the glycoluril trimers **TriMe** and **TriH** (Figure 5) were investigated. Based on our benchmarking of computational methods (Supporting Information, Tables S7, S8, S9, S10, S11), we employed the low-cost method B97-3c for geometry optimization and the accurate hybrid DFT functional PBE0 corrected for dispersion interactions (D3BJ) for final energy consideration. Both geometry and final energy calculations were performed in an implicit water environment provided by the SMD model. This model offers both polar and non-polar contributions to the solvation energies, and it is thus suitable for consideration of thermochemistry. The relative conformer stabilities obtained at the PBE0-D3BJ-SMD/def2-TZVPP//B97-3c-SMD level of theory are given in Table 1 (Supporting Information, Tables S12 and S13 contain detailed data). For **TriH**, the three forms were of nearly equal relative energy (**TriH**-F3: 0.0 kcal mol^{-1}; **TriH**-F2: 0.2 kcal mol^{-1}; **TriH**-F1: 0.6 kcal mol^{-1}) as expected based on literature precedent for the corresponding glycoluril dimers.

In sharp contrast, for **TriMe**, the three folded forms are predicted to be of very different energies (**TriMe**-F3: 5.1 kcal mol^{-1}; **TriMe**-F2: 3.5 kcal mol^{-1}; **TriMe**-F1: 0.0 kcal mol^{-1}). The lower stabilities of the F2 and F3 conformers of **TriMe** is caused by solvent and internal contributions, but the data obtained in vacuum (Supporting Information) indicate that steric factors also make a significant contribution. We believe that the steric bulk of the methyl groups on the central glycoluril of **TriMe** effectively dictates that the molecule folds into the **TriMe**-F1 form to avoid placing the Me-groups into the concavity of the adjacent glycoluril rings. Several aspects of the geometries of the different folded structures of **TriMe** and **TriH** are noteworthy. For example, a comparison of the terminal $H_3C{\bullet\bullet\bullet}CH_3$ distance d_{MM} for **TriH**-F1 is 9.231 Å, whereas the corresponding distance for **TriMe**-F1 is 8.978 Å. The shorter d_{MM} distance in **TriMe** arises from the increased curvature of the glycoluril trimer due to the presence of the methyl groups on the concave face. In contrast, the $H_3C{\bullet\bullet\bullet}CH_3$ distance for **TriH**-F3 is 9.724 Å, whereas the corresponding length for **TriMe**-F3 is increased to 13.841 Å. Rather than deforming by changing the curvature of the glycoluril trimer as observed for F1, the F3 folded form of **TriMe** releases the tension by an end-to-end twisting of the glycoluril trimer unit. This twisting was observed computationally for all structures. We quantified the twist by two dihedral angles, τ_1 and τ_2, describing the local (on the inverted glycoluril) and the global twist of glycoluril ribbon (Supporting Information, Tables S11 and S13; τ_2 is defined in Figure 5a). Due to the aforementioned steric factors, the global twist was found to be more pronounced for **TriMe**-F3 (τ_2 = 57.7°) than for **TriH**-F3 (τ_2 = 0.2°).

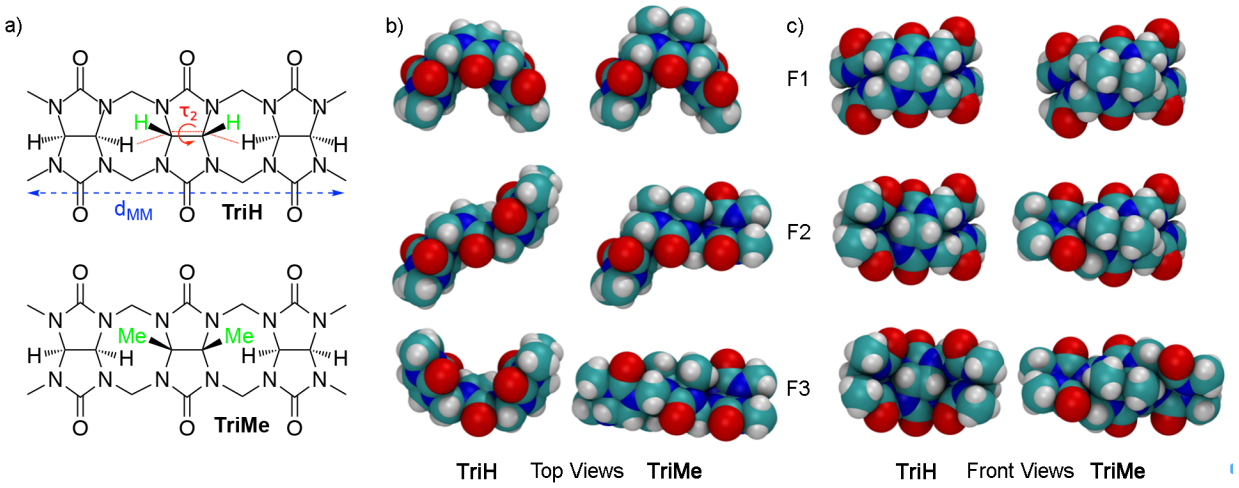

Figure 5. a) Chemical structures of **TriMe** and **TriH** with the definition of the terminal $H_3C\bullet\bullet\bullet CH_3$ distance d_{MM} and the global twist of glycoluril ribbon represented by a pseudo-dihedral angle τ_2. b) Top and c) front views of the geometries of the F1, F2, F3 conformers optimized at the B97-3c level of theory in implicit water (the back view is available in Figure S102).

Table 1. Relative conformer stabilities (E_r) for the investigated systems obtained at the PBE0-D3BJ/def2-TZVPP//B97-3c level of theory in the SMD model of implicit water. The relative energies E_r include contributions from the potential energy, as well as polar and non-polar solvation energies. Due to computational complexity, thermal contributions (vibration, rotation, and translation energies and entropies) were neglected. For each system, the most stable conformer has zero energy. All values are in kcal mol^{-1}.

	TriH	**TriMe**	**P1'**	**P2'**	**P1'·8**	**P2'·8**
Conf	**E_r**	**E_r**	**E_r**	**E_r**	**E_r**	**E_r**
F1	0.57	0.00	0.00	2.34	1.49	0.00
F2	0.22	3.45	3.05	4.11	2.87	2.98
F3	0.00	5.11	4.01	0.00	0.00	1.36

The use of glycoluril substituents as a conformational control element in this context is new.[27] Our intention is to use **P1** or **P2** as a host for alkylammonium ions via its F3 folded form,

which will require us to pay an energetic penalty to bias the conformational ensemble toward the **P1**-F3 or **P2**-F3 folded forms. Of course, the energetics of the F1 – F3 folded forms of **P1** and **P2** will be modified by the presence of the additional glycolurils and terminal aromatic rings which may bias the conformational ensemble toward the F3 form due to π–π interactions. To get at these questions, computational methods were employed. We used simplified models of **P1** and **P2** with removed solubilizing groups; these models are labeled as **P1'** and **P2'**. By this simplification, we tried to avoid possible problems with a not well-defined conformational preference of the flanking $O(CH_2)_3SO_3^-$ groups and the presence of negative charge (-4), which could be problematic for reliable DFT quantum chemical calculations. The computations of **P1'** and **P2'** were performed with the same methodology used for **TriMe** and **TriH** and the calculated relative conformational stabilities of **P1'** and **P2'** are provided in Table 1. In the case of **P1'**, calculations revealed conformational preferences very similar to **TriMe**. This indicates that the conformational preferences are mainly dictated by the presence of the double S-shaped central glycoluril rather than the aromatic sidewalls. Interactions between the aromatic side walls of **P1'** and the central methyl groups (**P1'**-F2) or with the second aromatic sidewall (π–π stacking, **P1'**-F3) were observed, but these interactions are not large enough to counterbalance other effects such as solvation (see Table S15 for energy decomposition). In the case of **P2'**, the difference between the F1 and F2 (+1.8 kcal mol^{-1}) forms is similar to that of **P1'** (+3.1 kcal mol^{-1}) or TriMe (+3.5 kcal mol^{-1}), but the **P2'**-F3 form is the lowest energy conformational form.

Figure 6 shows the minimized geometries of the **P2'**-F1, **P2'**-F2, and **P2'**-F3 conformations of host **P2'**; an analogous figure is given for **P1'** in the Supporting Information (Figure S103). In contrast to the idealized C_{2v}-symmetric line bond structures shown above in Figure 4, we observe more compact conformations for **P2'**-F2 and **P2'**-F3, presumably due to the

van der Waals interactions between the central Me-groups of **P2'** and the aromatic sidewall(s) in these conformations. For **P2'**-F3 (Figure 6a), we additionally observe offset π–π interactions between the faces of the naphthalene sidewalls. These interactions are responsible for the overall preference for F3 (0.0 kcal mol^{-1}) over F2 (4.1 kcal mol^{-1}) and F1 (2.3 kcal mol^{-1}). For guest binding to occur within **P2'**-F3, the disruption of these intramolecular non-covalent interactions must be counterbalanced by stronger host•guest non-covalent interactions. For critical assessment of the obtained results two additional contributions must be mentioned which are not available in our calculations. The first is the absence of thermal motions (mainly entropy) in the calculated energies. It can be expected that F3 will have lower entropy than F1 because its compact structure will limit movements of its aromatic walls (Figure S107 shows the dynamic behavior of aromatic walls in **P2•P2** dimer). This effect will decrease the stability of the F3 conformer relative to F1. Second, destabilizing electrostatic interactions between the negatively charged solubilizing groups would be expected to be larger for **P2**-F3 than for **P2**-F1.

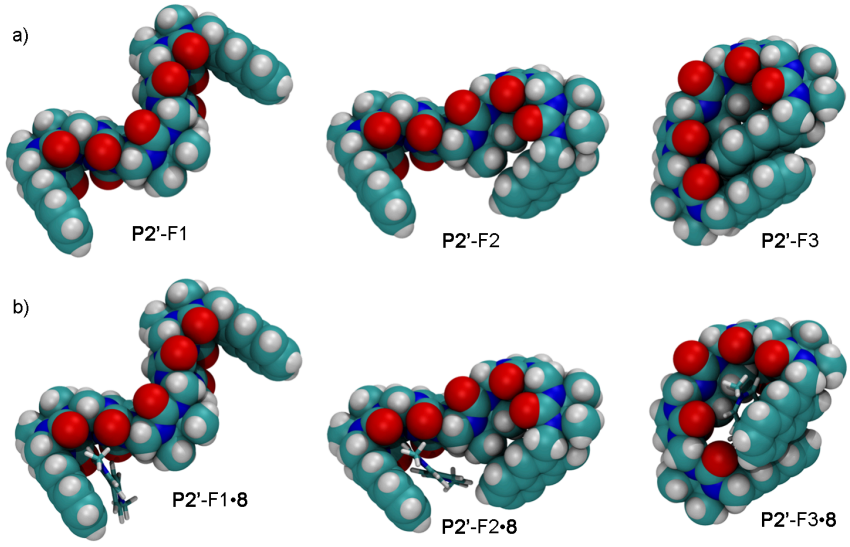

Figure 6. Structures of a) **P2'** (top line) and b) **P2'•8** (bottom line) in the F1, F2, and F3 folds obtained at the B97-3c level of theory in implicit water (see Figures S103-S106 for other views and structures for **P1'** and **P1'•8**).

Self-Association Studies Performed for P1 and P2. As a prelude to the planned host•guest binding studies, we investigated the self-association properties of **P1** and **P2** to ensure that the measured K_a values would not be influenced by host self-association.[28] Accordingly, we prepared solutions of **P1** and **P2** at their maximal solubility in D_2O and measured their ^1H NMR spectra as a function of [**P1**] or [**P2**] down to 0.12 mM. We did not observe any significant changes in the chemical shifts for **P1** over the 9 mM – 0.12 mM concentration range which indicates that **P1** does not undergo significant self-association (Supporting Information, Figure S24). Figure 7a shows the chemical shift of H_m as a function of [**P2**]. We fitted the change in chemical shift to a two-fold self-association model[29] which allowed us to extract the self-association constant of **P2** (K_s = 189 ± 27 M^{-1}). Because chemical exchange is fast on the NMR time scale, it is not possible to obtain precise information about the geometry of **P2•P2** from the NMR experiments. Accordingly, we performed molecular modelling; Figure 7b shows a representative snapshot of the **P2**-F1•**P2**-F1 dimer from a 1 μs long molecular dynamics simulation which is consistent with the observed upfield shifting of the H_a and H_b resonances of the aromatic sidewall and the resonance for $(CH_3)_m$ upon dimerization. The geometry of **P2•P2** depicted in Figure 7b is reminiscent of the geometry of dimeric molecular clips prepared by the Nolte and Isaacs groups which feature the aromatic sidewall of one molecule penetrating into the cleft of the opposing molecule and vice versa.[26] We also attempted to model the dimer from the **P2**-F2 form. However, soon after the start, both flanking side arms underwent conformation change into F1 (see Figure S108).

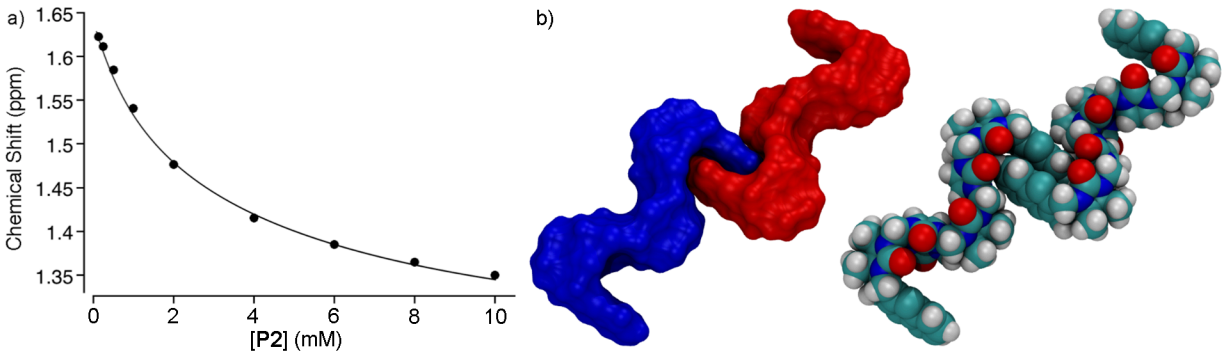

Figure 7. a) Plot of the chemical shift of H_m of **P2** as a function of [**P2**]. The solid line represents the best non-linear fitting of the data to a two-fold self-association model (K_s = 189 ± 27 M^{-1}). b) Two representations of the selected snapshot from MD simulation of **P2**-F1•**P2**-F1. Solubilizing groups were removed for clarity. Ensembles of overlapping snapshots for **P2**-F1•**P2**-F1 and **P2**-F2•**P2**-F2, including solubilizing groups, are provided in Figures S107 and S108.

Attempted Use of P1 and P2 as Solubilizing Excipients for Insoluble Drugs. Given our previous work on the use of acyclic CB[n]-type receptors as solubilizing excipients for insoluble drugs,[30] we initially tested the solubilization abilities of **P1** and **P2** toward a small panel of insoluble drugs (paclitaxel, fenofibrate, itraconazole, tamoxifen and ethynylestradiol, Figure 8). For this purpose, we separately prepared 7 mM solutions of **P1** and **P2** in 20 mM sodium phosphate buffered D_2O and dispensed the solution into a series of vials to which an excess of insoluble drug was added. After mixing overnight (16 h), the insolubles were removed by filtration through a 0.45 μm polyethersulfone membrane filter and the solution and a known volume of a solution of trimesic acid (1 mM) was transferred to an NMR tube for analysis. No drug solubilization was detected by ^{1}H NMR indicating that **P1** and **P2** are not promising candidates as solubilizing excipients for insoluble drugs.

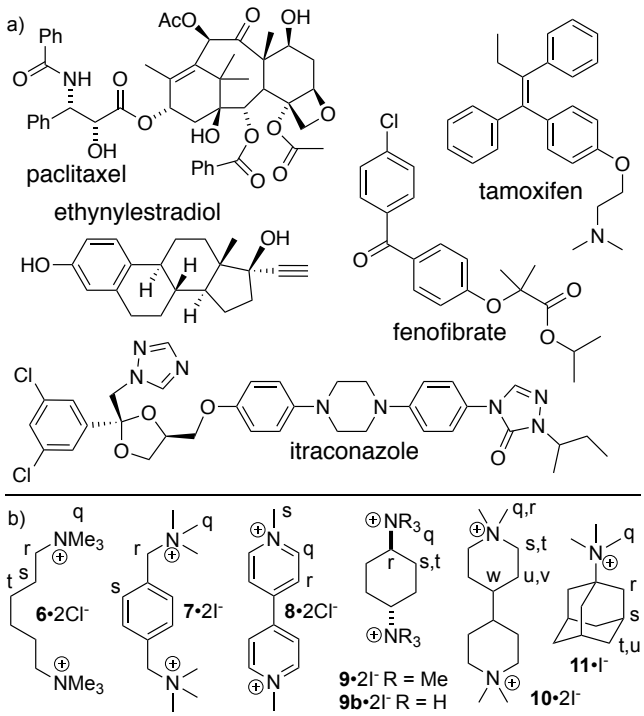

Figure 8. Structures of: a) insoluble drugs, and b) (di)cationic guests **6** – **11** used in this study.

Qualitative ^{1}H NMR Investigations of Host•Guest Recognition. In order to understand the poor solubilizing ability of **P1** and **P2** we decided to perform qualitative host•guest binding studies at 1:1 and 1:2 host:guest ratios. Initially, we attempted to prepare solutions of host **P1** (1 mM) and guests **7**, **9**, and **10** (≥ 2 mM) and observed the formation of precipitates indicating the poor solubility of the complexes. Similar observations were made for solutions of host **P2** (2 mM) and guests **7** – **9**. These problems can be avoided by working at lower concentrations of hosts **P1** and **P2** (e.g. 0.3 mM). It is not possible to reach saturation due to the low binding affinity for host•guest complexes of **P1** and **P2** (*vide infra*) and therefore experimentally observable complexation induced changes in chemical shift are small particularly for **P1**. For example, Figures 9a-c show the ^{1}H NMR spectra recorded for **8** (0.3 mM) and 1:1 and 1:2 mixtures of **P1** and **8** which exhibit upfield shifts of ≤ 0.2 ppm under these conditions. In contrast, Figure 10a-c shows the ^{1}H NMR spectra recorded for **8** (1.0 mM) and 1:1 and 1:2 mixtures of **P2** and **8**. Clear upfield shifting of

the aromatic H-atoms (H_q and H_r) of **8** upon complexation suggest the formation of a complex where the aromatic rings of guest **8** are located inside rather than on the exterior of host **P2**. The guest exchange processes were fast on the ^{1}H NMR chemical shift timescale which is expected when the host•guest complexes are relatively weak. The Supporting Information (Figures S26 – S43) shows the analogous ^{1}H NMR spectra recorded for guests **7 – 11** and hosts **P1** and **P2** which suggests the complexation of the central hydrophobic regions of guests **7** – **11** inside hosts **P1** and **P2** potentially in their **P1**-F3 and **P2**-F3 conformations.

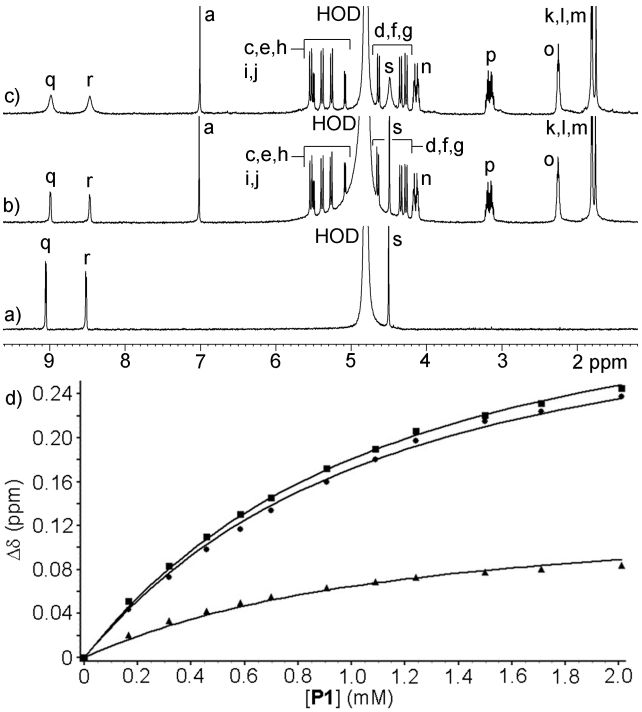

Figure 9. ^{1}H NMR spectra recorded (600 MHz, D_2O, RT) for: a) **8** (0.3 mM), b) a 1:1 mixture of **P1** (0.3 mM) and **8** (0.3 mM), and c) a 1:2 mixture of **P1** (0.3 mM) and **8** (0.6 mM). d) Plot of the absolute value of the change in chemical shifts of H_q (■), H_r (•), and H_s (▲) during the titration of **8** (0.3 mM) with **P1** (0 – 2.01 mM) in D_2O.

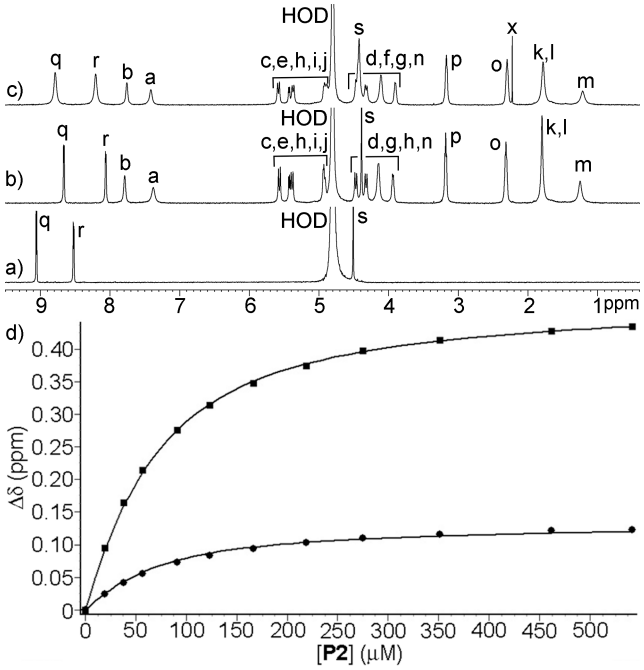

Figure 10. ^{1}H NMR spectra recorded (600 MHz, D_2O, RT) for: a) **8** (1.0 mM), b) a 1:1 mixture of **P2** (1.0 mM) and **8** (1.0 mM), and c) a 1:2 mixture of **P2** (1.0 mM) and **8** (2.0 mM). d) Plot of the absolute value of the change in chemical shifts of H_q (■) and H_s (•) during the titration of **8** (0.04 mM) with **P2** (0 – 0.541 mM) in D_2O.

Measurement of the Host•Guest Binding Constants. Initially, we attempted to measure the K_a values for the host•guest complexes by isothermal titration calorimetry (ITC). Unfortunately, under our usual conditions (20 mM sodium phosphate buffer, pH 7.4) very little heat was evolved and the data could not be fitted to a standard 1:1 binding model. Accordingly, we turned to ^{1}H NMR titrations. The titration of **8** (0.06 mM) with **P2** (0 – 0.96 mM) conducted in 20 mM sodium phosphate buffer (pH 7.4) again resulted in only very small changes in chemical shift of **8** which made clear that **P1** and **P2** were poor hosts. Therefore, we changed the medium to the less competitive unbuffered D_2O for determination of K_a values for **P1** and **P2**. Figure 9d shows the change in chemical shift of (H_q, H_r, and H_s) of a fixed concentration of guest **8** (0.3 mM) upon

titration with host **P1** (0 – 2.01 mM); the solid line represents the best fitting of the data to a 1:1 binding model implemented within Scientist^{TM} (Supporting Information) with $K_a = 1100 \pm 50$ M^{-1}. Similarly, Figure 10d shows the change in chemical shifts (H_q, H_s) of a fixed concentration of guest **8** (0.04 mM) recorded during the titration with host **P2** (0 – 541 μM). The solid line in Figure 10d represents the best non-linear least squares fit of the data to a binding model that takes into account the self-association of **P2** along with 1:1 host:guest binding (Supporting Information, page S70) with $K_a = 19800 \pm 400$ M^{-1}. Related titrations were performed for hosts **P1** and **P2** with guests **7** – **11** and are presented in the Supporting Information. The K_a values are collected in Table 2. From the fitting of ^{1}H NMR titrations data curves (Supporting Information) we were also able to extract the limiting chemical shifts of the **P1**•guest and **P2**•guest complexes and calculate the complexation induced changes in chemical shift (Δδ, Table 3). A perusal of Table 3 reveals that for the naphthalene walled hosts, the complexation induced changes in chemical shifts (Δδ) of guests are significantly larger for **Tet2** than for **P2**. Similarly, between the benzene walled hosts, the Δδ values are larger for **Tet1** than for **P1**. These disparities suggest that the geometry of the **P1**•guest and **P2**•guest complexes are not directly analogous to those of **Tet1** and **Tet2**. Accordingly, we wondered whether these weak binding processes might simply reflect electrostatic and hydrophobic interaction between the guest and the *outside* of the aromatic walls of the host or potentially to one of the clip-like cavities of **P1**-F1 or **P2**-F1. To test this possibility, we performed titrations between guests **6** – **11** and aromatic sidewalls **4** and **5** (Supporting Information). No changes in chemical shift were observed for mixtures of benzene derived wall **4** and guests **6** – **11**; accordingly no K_a values or Δδ values are reported in Tables 2 and 3 for wall **4**. For naphthalene wall **5** we did observe changes in chemical shift upon titration with guests **6** – **11**; we fitted those changes to a 1:1 binding model to obtain K_a values and Δδ values (Tables 2

and 3). The K_a values for the complexation between wall **5** and **6** – **11** are 6.7 – 23.6-fold weaker than between host **P2** and **6** – **11** and the Δδ values (Table 3) are much smaller for **5** than for **P2**. Based on this data we exclude the possibility that guests **6** – **11** simply bind to the exterior face of the aromatic sidewalls of host **P2**. The 1:1 stoichiometry of the **P2**•guest complexes was confirmed for guests **6**, **7**, and **10** by constructing Job plots (Supporting Information). The 1:1 stoichiometry suggests that the guest•**P2** complexes exist as the guest•**P2**-F3 conformer. For the very weak complexes between **P1** and guests **6** – **11** the Job plots were inconclusive with no clear maxima. The utility of Job plots has been called into question, especially for weak complexes studied under dilute conditions.[31] In addition to the Δδ values for the guest upon complexation, we also monitored the changes in **P2** chemical shift upon complexation with **6** – **11** (Supporting Information) and generally observe upfield shifts for H_g (≈ 0.3 ppm) and H_h (≈ 0.1 ppm) and a slight downfield shift (≤ 0.1 ppm) for H_e upon complexation. H_g and H_h are the diastereotopic protons on the methylene bridges involved in the S-shaped connections at the center of **P2**. The chemical shifts of the diastereotopic methylene bridges is CB[n] type hosts resonate at quite different chemical shifts due to the anisotropic effects of the ureidyl C=O group with the H-atoms nearer the lone pairs on oxygen appearing substantially downfield of those pointing away from the C=O groups. Accordingly, the significant upfield movement of H_g and H_h upon binding provides additional support for our conclusion that **P2** undergoes conformation change upon binding to yield the **P2**-F3•guest complexes.

Table 2. Binding constants (K_a, M^{-1}) measured for the different container•guest complexes.

	P1[a,e]	**P2**[a,e]	**5**[a,e]	**Tet1**[f]	**Tet2**[f]
6	$3.87 \pm 0.12 \times 10^2$	$7.71 \pm 0.22 \times 10^3$	$5.46 \pm 0.46 \times 10^2$	$8.93 \pm 0.33 \times 10^{7}$[b]	$4.59 \pm 0.09 \times 10^{8}$[c]

7	$1.40 \pm 0.03 \times 10^{3}$	$1.76 \pm 0.05 \times 10^{4}$	$7.47 \pm 2.14 \times 10^{2}$	$1.78 \pm 0.07 \times 10^{8}$[b]	$2.69 \pm 0.09 \times 10^{9}$[c]
8	$1.10 \pm 0.05 \times 10^{3}$	$1.98 \pm 0.04 \times 10^{4}$	$1.94 \pm 0.13 \times 10^{3}$	$4.69 \pm 0.22 \times 10^{8}$[b]	$2.14 \pm 0.09 \times 10^{9}$[c]
9	$9.00 \pm 0.40 \times 10^{2}$	$4.17 \pm 0.08 \times 10^{3}$	$6.21 \pm 0.64 \times 10^{2}$	$2.25 \pm 0.08 \times 10^{7}$[b]	$2.76 \pm 0.15 \times 10^{9}$[c]
10	$1.08 \pm 0.05 \times 10^{3}$	$5.12 \pm 0.12 \times 10^{3}$	$5.40 \pm 0.58 \times 10^{2}$	$3.09 \pm 0.24 \times 10^{6}$[d]	$1.30 \pm 0.03 \times 10^{10}$[c]
11	$3.75 \pm 0.24 \times 10^{2}$	$1.95 \pm 0.10 \times 10^{3}$	$2.70 \pm 0.83 \times 10^{2}$	$1.70 \pm 0.05 \times 10^{7}$[b]	$7.09 \pm 0.21 \times 10^{8}$[c]

[a] Measured by ^{1}H NMR titration. [b] Lit. values.[32] Measured by ITC competition assay using butan-1-amine as competitor in cell. [c] Measured by ITC competition assay using **9b** as competitor in cell. [d] Measured by direct ITC titration. [e] Measured in D_2O at RT. [f] Measured in 20 mM NaH_2PO_4 buffered H_2O (pH 7.4) at 298 K).

Table 3. Complexation induced changes in chemical shifts (Δδ) of guests obtained from the non-linear data fitting of the titration data for **P1**, **P2**, and wall **5** or directly from the ^{1}H NMR spectra for the tight binding complexes of **Tet1** and **Tet2**. For atom lettering see Figure 8.

Guest	Host	H_q Δδ	H_r Δδ	H_s Δδ	H_t Δδ	H_u Δδ	H_v Δδ	H_w Δδ
6	**Tet2**	0.50	1.17	1.37	1.32			
6	**5**	0.07	0.10	0.11	0.11			
6	**P2**	0.04	0.41	0.59	0.97			
6	**Tet1**	0.11	0.78	1.09	1.38			
6	**P1**	0.12	0.43	0.38	0.78			
7	**Tet2**	0.66	0.36	1.61				
7	**5**	0.07	0.16	0.15				
7	**P2**	0.18	0.34	0.76				
7	**Tet1**	0.17	0.72	1.27				
7	**P1**	0.08	0.17	0.29				
8	**Tet2**	1.05	1.56	0.30				
8	**5**	0.13	0.16	0.06				
8	**P2**	0.48	0.57	0.13				
8	**Tet1**	1.08	0.81	0.20				
8	**P1**	0.37	0.35	0.14				
9	**Tet2**	0.89	2.06	1.38	1.64			
9	**5**	0.05	0.20	0.11	0.12			
9	**P2**	0.16	0.50	0.41	0.53			
9	**Tet1**	0.88	0.81	0.91	1.08			
9	**P1**	0.27	0.79	0.62	0.67			
10	**Tet2**	0.34	0.77	1.02	1.28	1.44	1.47	1.09
10	**5**	0.07	0.10	0.16	0.18	0.19	0.20	0.24
10	**P2**	0.12	0.19	0.27	0.42	0.59	0.60	0.78
10	**Tet1**	0.25	0.45	0.60	0.77	0.96	0.89	1.17
10	**P1**	0.19	0.18	0.37	0.41	0.59	0.54	0.69
11	**Tet2**	0.42	1.62	1.90	1.16	1.5		
11	**5**	0.08	0.11	0.07	0.06	0.07		
11	**P2**	0.18	0.51	0.55	0.35	0.60		
11	**Tet1**	0.29	1.22	1.14	0.73	1.28		
11	**P1**	0.27	0.77	0.74	0.48	0.79		

Table 2 also presents the K_a values for complexes of **Tet1** with guests **6** – **11** measured previously by ITC in 20 mM sodium phosphate buffer (pH 7.4, RT) as a comparator for **P1**.[32] The logical comparator for **P2** is **Tet2**, but unfortunately, the K_a values for **Tet2** complexes with **6** – **11** were unknown. Accordingly, we measured the K_a values by isothermal titration calorimetry. We attempted direct ITC titrations but quickly found that the K_a values exceeded the dynamic range of the measurements (c-value > 300).[33] Accordingly, we decided to perform competition ITC.[34] In competition ITC, a host and an excess of a weak binding guest of known K_a and ΔH is titrated with an excess of a stronger binding guest; fitting of the data to a competition binding model then allows extraction of the K_a and ΔH values for the tighter binding complex. Figure 11a shows the thermogram for the titration of a mixture of host **Tet2** (105 μM) and *trans*-1,4-diamino cyclohexane dihydrochloride (**9b**, 750 μM) as competitor in the cell with guest **9** (1.0 mM) in the syringe. Figure 11b shows a plot of the integrated heats versus the **Tet2**:**9** molar ratio fitted to a competition binding model in the PEAQ-ITC data analysis software which allowed the determination of the strength of the **Tet2•9** complex ($K_a = 2.76 \times 10^9$ M^{-1}; $\Delta H = -13.3$ kcal mol^{-1}). Table 2 reports the binding constants for the **Tet2•**guest complexes by competition ITC and the data is given in the Supporting Information.

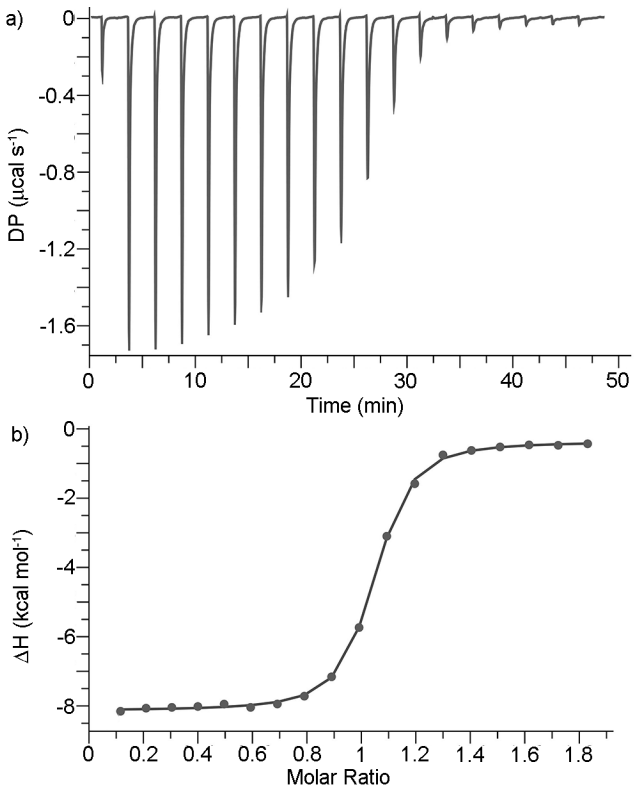

Figure 11. a) ITC thermogram from the titration of a mixture of **Tet2** (105 mM) and competitor **9b** (750 μM) in the cell with guest **9** (1.0 mM) in the syringe. b) Plot of ΔH versus molar ratio used to extract K_a and ΔH for **Tet2•9**.

Modelling of the Conformations of Host-Guest Complexes.

The optimized structures of the pentamers **P1'** and **P2'** (Figure 6) were used to model the complexes with guest **8**. In the case of F3, we inserted the guest **8** into an artificially created cavity. The structures obtained for **P2'•8** fully optimized in implicit water are summarized in Figure 6 whereas the analogously obtained structures of **P1'•8** are shown in Figure S105. In the F1 and F2 forms, guest **8** binds into the clip-like cavity. In the case of F3, the aromatic walls undergo an out-of-plane twisting and reorganization to maximize contact with the guest, and as a result, they no longer π–π stack with each other anymore. For **P1** and **P2** which bear $O(CH_2)_3SO_3^-$ solubilizing

groups, there may be steric interactions or electrostatic interactions between solubilizing groups, and it can be expected that the computationally obtained complexes with the **P1'** and **P2'** hosts in the F3 conformational state may not fully represent the real situation. The computed relative stabilities of the complexes of **8** with **P1'** and **P2'** (Table 1) revealed that the most stable conformer is F3 for **P1'•8** and F1 for **P2'•8**. This indicates that the preference for conformational states can change during the binding. Similar to the free hosts, two contributions were not included in our analysis, the thermal motions (entropy) and impact solubilizing groups, which may have a destabilizing effect on the complexes in the F3 conformational state as discussed above.

Discussion of the Trends in the Binding Constants. An examination of the K_a values in Table 2 reveal a number of significant trends. First, both **P1** and **P2** are relatively poor hosts with the K_a values for the series of (di)ammonium ions (**6** – **11**) – generally excellent guests for CB[n]-type receptors – ranging from 375 to 1400 M^{-1} for **P1** and from 1950 to 19800 M^{-1} for **P2**. Amongst guests **6** – **11**, guests **7** and **8** which contain aromatic rings bind most tightly to **P1** and **P2**, presumably due to π–π interactions in the complexes. Second, **P2** is always a better host than **P1** toward **6** – **11** with ratios of K_a values as follows: **6** (19.9-fold), **7** (12.6-fold), **8** (18-fold), **9** (4.6-fold), **10** (4.7-fold), **11** (5.2-fold). We believe that **P2** is a slightly better host than **P1** due to either a larger population of the F3 conformer or the larger π-surfaces of **P2** which form stronger non-covalent interactions with guests, or a combination of the two. Similarly, a comparison of the K_a values of **Tet2** and **Tet1** toward **6** – **11** shows that **Tet2** is uniformly the superior host (**6** (5.1-fold), **7** (15-fold), **8** (4.5-fold), **9** (123-fold), **10** (4200-fold), **11** (42-fold)). Related trends have been seen previously for the complexes of **Tet1** and **Tet2** toward insoluble drugs and neuromuscular blocking agents.[19,30] We attributed these trends to the potential for augmented π–π interactions

with the naphthalene walled hosts **Tet2** and **P2**. For hosts **Tet1** and **Tet2** the selectivity is largest for the bulkier alicyclic guests **9** – **11** and smallest for the narrow aliphatic guest **6** which suggests that smaller host **Tet1** must undergo energetically costly cavity expansion to accommodate the larger guests. The narrow dynamic range of K_a values for hosts **P1** and **P2** does not allow us to draw any firm conclusions regarding guest size preference. Previously, we have observed that **Tet1** is a more potent host than **Tri1** and that **Tet2** is a more potent host than **Tri2**.[23] The data in Table 2 allows an analogous comparison of **P1** with **Tet1** and **P2** with **Tet2**. We find that **Tet1** is a substantially better host than **P1** toward guests **6** – **11** (**6**: 2.3×10^5-fold, **7**: 1.3×10^5-fold, **8**: 4.3×10^5-fold, **9**: 2.5×10^4-fold, **10**: 2.9×10^3-fold, **11**: 4.5×10^4-fold) and that **Tet2** is far superior than **P2** (**6**: 6.0×10^4-fold, **7**: 1.5×10^5-fold, **8**: 1.1×10^5-fold, **9**: 6.6×10^5-fold, **10**: 2.5×10^6-fold, **11**: 3.6×10^5-fold). Overall, the binding data shows that **P1** and **P2** are relatively poor hosts toward hydrophobic (di)cations **6** – **11** which are generally excellent guests for CB[n]-type hosts. We surmise that the poor performance of **P1** and **P2** is because the uncomplexed hosts must undergo an energetically costly folding process to populate the **P1**-F3 and **P2**-F3 conformation before guest binding (Figure 6).

Conclusions. In summary, we have described the synthesis of an important new glycoluril oligomer building block (S-shaped pentamer **3**) and its transformation into two new acyclic CB[n]-type receptors **P1** and **P2**. Hosts **P1** and **P2** have moderate solubility in water (≈ 9 and ≈ 11 mM); **P1** does not self-associate whereas **P2** undergoes only weak intermolecular self-association (K_s = 189 ± 27 M^{-1}). **P1** and **P2** are relatively poor hosts toward (di)cationic guests **6** – **11** as established by ^{1}H NMR titrations (**P1**: 375 to 1400 M^{-1}; **P2**: 1950 to 19800 M^{-1}). Host **P2** with its larger naphthalene rings is the more potent host in all cases relative to **P1**. In sharp contrast, guests **6** –

11 form much tighter complexes (10^3 – 10^6 fold) with acyclic CB[n] based on glycoluril tetramers (**Tet1** and **Tet2**). The relatively poor recognition abilities of **P1** and **P2** are traced to their ability to adopt three conformational isomers around their S-shaped segments (F1 – F3). For **P1** there is a computational derived preference for the F1-fold (**TriMe**-F3: +5.1 kcal mol^{-1}; **P1'**-F3: +4.0 kcal mol^{-1}) whereas for **P2** there is a smaller preference for the F3-fold (**P2'**-F1: +2.3 kcal mol^{-1}). The need to pay the energetic cost to shift the conformational equilibrium toward the F3-folded forms of **P1** and induce cavity formation in the F3-folded forms of **P1** and **P2** required for 1:1 host:guest cavity binding results in the observed low K_a values. Interestingly, calculations performed for **TriH** show no preference for the F1-fold which suggests that the Me-substituents play a major steric role in biasing the F1 – F3 equilibrium. In turn, this observation opens up the use of substituted glycolurils as building blocks to rationally design S-shaped glycoluril oligomers with well-defined conformational ensembles. In conclusion, these results highlight the importance of controlling the ensemble of conformations open to a host (e.g. maximizing host pre-organization) and minimizing host self-complexation when attempting to maximize host•guest binding affinity.

Computational Details.

The relative stabilities of the F1, F2, and F3 conformers were investigated on simplified models employing density functional theory (DFT) approach. These models included **TriMe** and **TriH** containing two S-shaped connections between adjacent glycolurils, models **P1'** and **P2'** with solubilizing groups ($O(CH_2)_3SO_3Na$) absent representing simplified versions of **P1** and **P2**, and complexes of **P1'** and **P2'** with guest **8**. Initial structures were built *in silico* in the three conformational states and then their geometries were optimized employing B97-3[35] method in an implicit water described by the SMD[36] model. Finally, the relative stabilities were evaluated at the

PBE0-D3BJ/def2-TZVPP level of theory[37] in the SMD implicit water on the optimized geometries. The employed computational methodology was thoroughly tested and showed similar accuracy as MP2/CBS. Further computational details, optimized geometries, and their absolute energies are available in the Supporting Information. All quantum chemical calculations presented in the main text were performed in Orca 4.2.1.[38]

A possible structure of the **P2•P2** dimer was investigated by molecular dynamics simulations performed in the Amber 16 package.[39] The **P2** host was considered in the F1 and F2 folds, which resulted in two possible dimeric structures (**P2**-F1•**P2**-F1 and **P2**-F2•**P2**-F2). These dimers were built *in silico* and described by the GAFF force field in MD simulations.[40] Each dimer was immersed into a box filled by an explicit water solvent described the TIP3P model with electroneutrality maintained by 8 sodium cations. In total, each system was simulated for 1 μs at a temperature of 300 K and a pressure of 100 kPa.

Experimental Details. Compounds **4** and **5** were prepared according to the literature procedures.[24] NMR spectra were measured on 400 MHz, 500 MHz, 600, and 800 MHz spectrometers (400, 500, 600, 800 MHz for ^{1}H NMR; 126 MHz for ^{13}C NMR) at room temperature in the stated deuterated solvents.

Compound 3. Glycoluril **1** (4.78 g, 33.6 mmol) was dissolved in 90% aq. methanesulfonic acid (80 mL). Then the solution was cooled to 8-12 °C using an ice bath within 20 min. and **2** (15.97 g, 62.8 mmol) was added in one portion and the reaction was stirred at 8-12 °C for 2 h and then 2 h at room temperature. The reaction mixture was poured into acetone (1.4 L) that had been cooled in ice for 30 min. to give a precipitate which was obtained by filtration. The crude solid was

washed with ethanol. The crude solid was then dissolved in acetonitrile/water (1:1 v:v, 200 mL) and stored in the refrigerator for 2-3 days. The resulting precipitate was isolated by filtration and then purified by successive cycles of stirring and centrifuging using the following solvent series: DMSO (6 mL), H_2O (12 mL), CH_3CN/H_2O 1:1 (20 mL), acetone (30 mL), Et_2O (30 mL). The final off-white residue was dried under high vacuum to give **3** (847 mg, 5%). M.p. > 300 °C. IR (ATR, cm^{-1}): 2917w, 2849w, 1711s, 1452s, 1371m, 1308m, 1250m, 1224m, 1187m, 1079m, 1012w, 958w, 918w, 862w, 770m. ^{1}H NMR (DMSO-d_6, 800 MHz, 30 °C): 5.54 (d, J = 15.2, 4H), 5.51 (d, J = 8.6, 2H), 5.21 (d, J = 13.7, 4H), 5.16 (d, J = 11.0, 4H), 5.09 (d, J = 8.6, 2H), 4.86 (d, J = 11.0, 4H), 4.71 (d, J = 13.7, 4H), 4.27 (d, J = 15.2, 4H), 1.82 (s, 6H), 1.70 (s, 6H), 1.64 (s, 6H).^{13}C NMR (DMSO- d_6, 126 MHz, 30 °C): 154.7, 154.7, 153.8, 78.00, 77.0, 72.4, 70.6, 69.5, 62.4, 48.2, 47.5, 17.8, 16.6, 15.8. HR-MS (ESI): *m/z* 1091.4953 ([M + hexanediamine + H]$^+$), $C_{44}H_{63}N_{22}O_{12}$, calculated 1091.4996; 546.2520 ([M + hexanediammonium]$^{2+}$), $C_{44}H_{64}N_{22}O_{12}$, calculated 546.2532.

Host P1. Compound **3** (1.57 g, 1.60 mmol) was charged to a round bottomed flask followed by trifluoroacetic acid (5.1 mL), Ac_2O (5.1 mL), and then finally **4** (1.47 g, 3.68 mmol) was added. The reaction mixture was stirred and heated at 75 °C for 3 h. The reaction mixture was poured into MeOH (65 mL) and the resulting precipitate was isolated by filtration. The crude solid was triturated with boiling water (30 mL) and then cooled in the refrigerator. The resulting solid was collected by centrifugation, dissolved in water and adjusted to pH 7 with 1 M aqueous NaOH. The solution was filtered to remove dust and then concentrated to dryness by rotary evaporation to afford host **P1** as an off-white solid (597 mg, 22%). M.p. > 300 °C. IR (ATR, cm^{-1}): 3427m, 2944w, 1703s, 1460s, 1374m, 1311m, 1182s, 1081m, 1036s, 844w, 796w, 786w. ^{1}H NMR

(DMSO-d_6, 400 MHz, 30 °C): 6.84 (s, 4H), 5.50 (d, *J* = 15.9 Hz, 4H), 5.41 (d, *J* = 8.6 Hz, 2H), 5.28 (d, *J* = 16.2 Hz, 4H), 5.13 (d, *J* = 13.8 Hz, 4H), 5.05 (d, *J* = 8.6 Hz, 2H), 4.59 (d, *J* = 13.8 Hz, 4H), 4.17 (d, *J* = 15.9 Hz, 4H), 4.13 (d, *J* = 16.2 Hz, 4H), 4.00 - 3.93 (m, 8H), 2.69 – 2.56 (m, 8H), 2.03 - 1.97 (m, 8H), 1.73 (s, 6H), 1.67 (s, 6H), 1.60 (s, 6H). ^{13}C NMR (D_2O, 126 MHz, 30°C, dioxane as internal reference): 157.3, 157.1, 156.5, 150.7, 128.6, 115.6, 80.0, 79.7, 78.3, 71.6, 69.4, 64.4, 49.4, 48.7, 48.3, 35.6, 25.2, 16.5, 16.2, 15.4. HR-MS (ESI): *m/z* 547.8031 ($[M-H]^{3-}$), $C_{62}H_{75}N_{20}O_{26}S_4$, calculated 547.8020; 410.5995 ($[M-H]^{4-}$), $C_{62}H_{74}N_{20}O_{26}S_4$, calculated 410.5997.

Host P2. A round bottomed flask was charged with **3** (976 mg, 1.00 mmol), trifluoroacetic acid (3.2 mL), Ac_2O (3.2 mL), and then finally **5** (1.01 g, 2.3 mmol). The reaction mixture was stirred and heated at 75 °C for 3 h. The reaction mixture was poured into MeOH (50 mL) and the precipitate was isolated by filtration. The crude solid was dissolved in water (25 mL) and precipitated by the addition of KCl (900 mg, 12.0 mmol). The precipitate was isolated by centrifugation and then dissolved in water and adjusted to pH 7 with 1 M aqueous NaOH. The solution was filtered to remove dust and then concentrated to dryness by rotary evaporation to afford **P2** as a pale yellow solid (492 mg, 27%). M.p. > 300 °C. IR (ATR, cm^{-1}): 3421w, 2999w, 2979w, 2944w, 1707s, 1458s, 1373m, 1311m, 1225m, 1183s, 1079m, 1034m, 950w, 785w, 757w. ^{1}H NMR (DMSO-d_6, 400 MHz, 30 °C): 7.99 (m, 4H), 7.56 (m, 4H), 5.51 (d, *J* = 15.5 Hz, 4H), 5.38 (d, *J* = 8.7 Hz, 2 H), 5.34 (d, *J* = 15.8 Hz, 4H), 5.06 (d, *J* = 13.9 Hz, 4H), 4.97 (d, *J* = 8.7 Hz, 2H), 4.51 (d, *J* = 13.9 Hz, 4H), 4.41 (d, *J* = 15.8, 4H), 4.22 - 4.18 (m, 4H), 4.16 (d, *J* = 15.5 Hz, 4H), 3.93- 3.91 (m, 4H), 2.77 – 2.73 (m, 8H), 2.18 – 2.15 (m, 8H), 1.76 (s, 12H), 1.63 (s, 6H). ^{13}C NMR (D_2O, 126 MHz, 30 °C, dioxane as internal reference): 157.0, 156.7, 156.1, 148.9, 128.1, 127.3, 127.0, 122.9, 79.7, 79.3, 78.1, 74.8, 71.4, 64.2, 49.2, 48.6, 48.2, 36.8, 25.8, 16.4, 16.1, 15.9.

HR-MS (ESI): *m/z* 872.2222 ($[M-H]^{2-}$), $C_{70}H_{80}N_{20}O_{26}S_4$, calculated 872.2223; 581.1456 ($[M-H]^{3-}$), $C_{70}H_{79}N_{20}O_{26}S_4$, calculated 581.1458; 435.6078 ($[M-H]^{4-}$), $C_{70}H_{78}N_{20}O_{26}S_4$, calculated 435.6075.

Disclosure Statement. L.I. is an inventor on patents related to the use of acyclic cucurbiturils in biomedical applications.

Funding. L.I. thanks the National Science Foundation (CHE-1404911) and the National Institutes of Health (CA-168365 and GM-132345) for financial support. V.S. thanks RECETOX Research Infrastructure (LM2015051 and CZ.02.1.01/0.0/0.0/16_013/0001761) for financial support. P.K. acknowledges computational resources provided by the CESNET LM2015042, the CERIT Scientific Cloud LM2015085, and the IT4Innovations National Supercomputing Center LM2015070 under the program "Large Infrastructures for Research, Experimental Development and Innovations" by the Ministry of Education, Youth and Sports of the Czech Republic. P.K. thanks the Ministry of Education, Youth and Sports of the Czech Republic under the National Sustainability Programme II for financial support (Project CEITEC 2020 (LQ1601)).

Table of Contents Graphic:

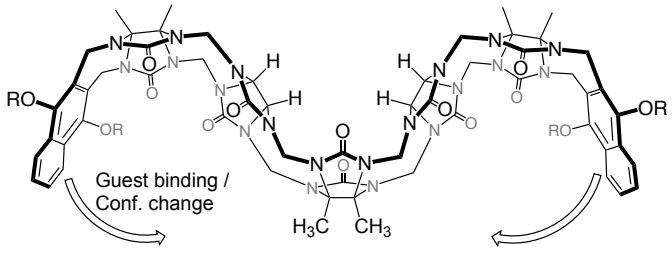

References.

1) Kim, J.; Jung, I.-S.; Kim, S.-Y.; Lee, E.; Kang, J.-K.; Sakamoto, S.; Yamaguchi, K.; Kim, K. *J. Am. Chem. Soc.* **2000**, *122*, 540-541; Day, A. I.; Arnold, A. P.; Blanch, R. J.; Snushall, B. *J. Org. Chem.* **2001**, *66*, 8094-8100; Day, A. I.; Blanch, R. J.; Arnold, A. P.; Lorenzo, S.; Lewis, G. R.; Dance, I. *Angew. Chem. Int. Ed.* **2002**, *41*, 275-277; Liu, S.; Zavalij, P. Y.; Isaacs, L. *J. Am. Chem. Soc.* **2005**, *127*, 16798-16799; Cheng, X.-J.; Liang, L.-L.; Chen, K.; Ji, N.-N.; Xiao, X.; Zhang, J.-X.; Zhang, Y.-Q.; Xue, S.-F.; Zhu, Q.-J.; Ni, X.-L.; Tao, Z. *Angew. Chem. Int. Ed.* **2013**, *52*, 7252-7255.
2) Freeman, W. A.; Mock, W. L.; Shih, N.-Y. *J. Am. Chem. Soc.* **1981**, *103*, 7367-7368; Lee, J. W.; Samal, S.; Selvapalam, N.; Kim, H.-J.; Kim, K. *Acc. Chem. Res.* **2003**, *36*, 621-630.
3) Mock, W. L.; Shih, N.-Y. *J. Org. Chem.* **1986**, *51*, 4440-4446.
4) Liu, S.; Ruspic, C.; Mukhopadhyay, P.; Chakrabarti, S.; Zavalij, P. Y.; Isaacs, L. *J. Am. Chem. Soc.* **2005**, *127*, 15959-15967; Rekharsky, M. V.; Mori, T.; Yang, C.; Ko, Y. H.; Selvapalam, N.; Kim, H.; Sobransingh, D.; Kaifer, A. E.; Liu, S.; Isaacs, L.; Chen, W.; Moghaddam, S.; Gilson, M. K.; Kim, K.; Inoue, Y. *Proc. Natl. Acad. Sci. U. S. A.* **2007**, *104*, 20737-20742; Cao, L.; Sekutor, M.; Zavalij, P. Y.; Mlinaric-Majerski, K.; Glaser, R.; Isaacs, L. *Angew. Chem. Int. Ed.* **2014**, *53*, 988-993; Jeon, W. S.; Moon, K.; Park, S. H.; Chun, H.; Ko, Y. H.; Lee, J. Y.; Lee, E. S.; Samal, S.; Selvapalam, N.; Rekharsky, M. V.; Sindelar, V.; Sobransingh, D.; Inoue, Y.; Kaifer, A. E.; Kim, K. *J. Am. Chem. Soc.* **2005**, *127*, 12984-12989.
5) Biedermann, F.; Uzunova, V. D.; Scherman, O. A.; Nau, W. M.; De Simone, A. *J. Am. Chem. Soc.* **2012**, *134*, 15318-15323; Biedermann, F.; Nau, W. M.; Schneider, H.-J. *Angew. Chem. Int. Ed.* **2014**, *53*, 11158-11171; Nau, W. M.; Florea, M.; Assaf, K. I. *Isr. J. Chem.* **2011**, *51*, 559-577.
6) Isaacs, L. *Acc. Chem. Res.* **2014**, *47*, 2052-2062; Del Barrio, J.; Horton, P.; Lairez, D.; Lloyd, G.; Toprakcioglu, C.; Scherman, O. *J. Am. Chem. Soc.* **2013**, *135*, 11760-11763; del Barrio, J.; Ryan, S. T. J.; Jambrina, P. G.; Rosta, E.; Scherman, O. A. *J. Am. Chem. Soc.* **2016**, *138*, 5745-5748.
7) Ko, Y. H.; Kim, E.; Hwang, I.; Kim, K. *Chem. Commun.* **2007**, 1305-1315.
8) Ghale, G.; Nau, W. M. *Acc. Chem. Res.* **2014**, *47*, 2150-2159; Barrow, S. J.; Kasera, S.; Rowland, M. J.; del Barrio, J.; Scherman, O. A. *Chem. Rev.* **2015**, *115*, 12320-12406; Masson, E.; Ling, X.; Joseph, R.; Kyeremeh-Mensah, L.; Lu, X. *RSC Adv.* **2012**, *2*, 1213-1247; Wheate, N. J.; Limantoro, C. *Supramol. Chem.* **2016**, *28*, 849-856.
9) Park, K. M.; Murray, J.; Kim, K. *Acc. Chem. Res.* **2017**, *50*, 644-646; Kim, E.; Kim, D.; Jung, H.; Lee, J.; Paul, S.; Selvapalam, N.; Yang, Y.; Lim, N.; Park, C. G.; Kim, K. *Angew. Chem., Int. Ed.* **2010**, *49*, 4405-4408; Cao, L.; Hettiarachchi, G.; Briken, V.; Isaacs, L. *Angew. Chem. Int. Ed.* **2013**, *52*, 12033-12037; Chen, H.; Ma, H.; Tan, Y. *J. Polym. Sci., Part A: Polym. Chem.* **2015**, *53*, 1748-1752; Yeom, J.; Kim, S. J.; Jung, H.; Namkoong, H.; Yang, J.; Hwang, B. W.; Oh, K.; Kim, K.; Sung, Y. C.; Hahn, S. K. *Adv. Healthcare Mater.* **2015**, *4*, 237-244; Webber, M. J.; Appel, E. A.; Vinciguerra, B.; Cortinas, A. B.; Thapa, L. S.; Jhunjhunwala, S.; Isaacs, L.; Langer, R.; Anderson, D. G. *Proc. Natl. Acad. Sci. U. S. A.* **2016**, *113*, 14189-14194; Zou, L.; Braegelman, A. S.; Webber, M. J. *ACS Cent. Sci.* **2019**, *5*, 1035-1043; Chen, H.; Huang, Z.; Wu, H.; Xu, J.-F.; Zhang, X. *Angew. Chem., Int. Ed.* **2017**, *56*, 16575-16578; Samanta, S. K.; Quigley, J.; Vinciguerra, B.; Briken, V.; Isaacs, L. *J. Am. Chem. Soc.* **2017**, *139*, 9066-9074; Sasmal, R.; Das Saha, N.; Pahwa, M.; Rao, S.; Joshi, D.; Inamdar, M. S.; Sheeba, V.; Agasti, S. S. *Anal. Chem.* **2018**, *90*, 11305-11314; Sun, C.; Zhang, H.; Li, S.; Zhang, X.; Cheng, Q.; Ding, Y.; Wang, L.-H.; Wang, R. *ACS Appl. Mater. Interfaces* **2018**, *10*, 25090-25098.

10) Witt, D.; Lagona, J.; Damkaci, F.; Fettinger, J. C.; Isaacs, L. *Org. Lett.* **2000**, *2*, 755-758; Chakraborty, A.; Wu, A.; Witt, D.; Lagona, J.; Fettinger, J. C.; Isaacs, L. *J. Am. Chem. Soc.* **2002**, *124*, 8297-8306; Lagona, J.; Fettinger, J. C.; Isaacs, L. *Org. Lett.* **2003**, *5*, 3745-3747.
11) Wu, A.; Chakraborty, A.; Witt, D.; Lagona, J.; Damkaci, F.; Ofori, M. A.; Chiles, J. K.; Fettinger, J. C.; Isaacs, L. *J. Org. Chem.* **2002**, *67*, 5817-5830.
12) Stancl, M.; Hodan, M.; Sindelar, V. *Org. Lett.* **2009**, *11*, 4184-4187.
13) Stancl, M.; Gargulakova, Z.; Sindelar, V. *J. Org. Chem.* **2012**, *77*, 10945-10948.
14) Huang, W.-H.; Zavalij, P. Y.; Isaacs, L. *J. Am. Chem. Soc.* **2008**, *130*, 8446-8454.
15) Isaacs, L.; Park, S.-K.; Liu, S.; Ko, Y. H.; Selvapalam, N.; Kim, Y.; Kim, H.; Zavalij, P. Y.; Kim, G.-H.; Lee, H.-S.; Kim, K. *J. Am. Chem. Soc.* **2005**, *127*, 18000-18001.
16) Ganapati, S.; Isaacs, L. *Isr. J. Chem.* **2018**, *58*, 250-263.
17) Stancl, M.; Gilberg, L.; Ustrnul, L.; Necas, M.; Sindelar, V. *Supramol. Chem.* **2014**, *26*, 168-172.
18) Lu, X.; Samanta, S. K.; Zavalij, P. Y.; Isaacs, L. *Angew. Chem., Int. Ed.* **2018**, *57*, 8073-8078; Mao, D.; Liang, Y.; Liu, Y.; Zhou, X.; Ma, J.; Jiang, B.; Liu, J.; Ma, D. *Angew. Chem. Int. Ed.* **2017**, *41*, 12614-12618; Jiang, S.; Lan, S.; Mao, D.; Yang, X.; Shi, K.; Ma, D. *Chem. Commun.* **2018**, *54*, 9486-9489; Mao, W.; Mao, D.; Yang, F.; Ma, D. *Chem. - Eur. J.* **2019**, *25*, 2272-2280; Bauer, D.; Andrae, B.; Gass, P.; Trenz, D.; Becker, S.; Kubik, S. *Org. Chem. Front.* **2019**, Ahead of Print.
19) Ma, D.; Zhang, B.; Hoffmann, U.; Sundrup, M. G.; Eikermann, M.; Isaacs, L. *Angew. Chem. Int. Ed.* **2012**, *51*, 11358-11362.
20) Hoffmann, U.; Grosse-Sundrup, M.; Eikermann-Haerter, K.; Zaremba, S.; Ayata, C.; Zhang, B.; Ma, D.; Isaacs, L.; Eikermann, M. *Anesthesiology* **2013**, *119*, 317-325; Haerter, F.; Simons, J. C. P.; Foerster, U.; Moreno Duarte, I.; Diaz-Gil, D.; Ganapati, S.; Eikermann-Haerter, K.; Ayata, C.; Zhang, B.; Blobner, M.; Isaacs, L.; Eikermann, M. *Anesthesiology* **2015**, *123*, 1337-1349.
21) Ganapati, S.; Grabitz, S. D.; Murkli, S.; Scheffenbichler, F.; Rudolph, M. I.; Zavalij, P. Y.; Eikermann, M.; Isaacs, L. *ChemBioChem* **2017**, *18*, 1583-1588.
22) Zhang, X.; Xu, X.; Li, S.; Li, L.; Zhang, J.; Wang, R. *Theranostics* **2019**, *9*, 633.
23) Gilberg, L.; Zhang, B.; Zavalij, P. Y.; Sindelar, V.; Isaacs, L. *Org. Biomol. Chem.* **2015**, *13*, 4041-4050.
24) Ma, D.; Hettiarachchi, G.; Nguyen, D.; Zhang, B.; Wittenberg, J. B.; Zavalij, P. Y.; Briken, V.; Isaacs, L. *Nat. Chem.* **2012**, *4*, 503-510.
25) Sijbesma, R. P.; Kentgens, A. P. M.; Lutz, E. T. G.; van der Maas, J. H.; Nolte, R. J. M. *J. Am. Chem. Soc.* **1993**, *115*, 8999-9005.
26) Rowan, A. E.; Elemans, J. A. A. W.; Nolte, R. J. M. *Acc. Chem. Res.* **1999**, *32*, 995-1006; Wu, A.; Chakraborty, A.; Fettinger, J. C.; Flowers, R. A., II; Isaacs, L. *Angew. Chem. Int. Ed.* **2002**, *41*, 4028-4031; Burnett, C. A.; Witt, D.; Fettinger, J. C.; Isaacs, L. *J. Org. Chem.* **2003**, *68*, 6184-6191.
27) Wu, F.; Wu, L.-H.; Xiao, X.; Zhang, Y.-Q.; Xue, S.-F.; Tao, Z.; Day, A. I. *J. Org. Chem.* **2012**, *77*, 606-611; Zhao, Y.; Mandadapu, V.; Iranmanesh, H.; Beves, J. E.; Day, A. I. *Org. Lett.* **2017**, *19*, 4034-4037.
28) Diederich, F. *Angew. Chem., Intl. Ed. Engl.* **1988**, *27*, 362-386.
29) Isaacs, L.; Witt, D.; Fettinger, J. C. *Chem. Commun.* **1999**, 2549-2550; Wu, A.; Mukhopadhyay, P.; Chakraborty, A.; Fettinger, J. C.; Isaacs, L. *J. Am. Chem. Soc.* **2004**, *126*, 10035-10043.
30) Zhang, B.; Isaacs, L. *J. Med. Chem.* **2014**, *57*, 9554-9563.

31) Hibbert, D. B.; Thordarson, P. *Chem. Commun.* **2016**, *52*, 12792-12805.
32) Xue, W.; Zavalij, P. Y.; Isaacs, L. *Org. Biomol. Chem.* **2019**, *17*, 5561-5569.
33) Wiseman, T.; Williston, S.; Brandts, J. F.; Lin, L.-N. *Anal. Biochem.* **1989**, *179*, 131-137; Broecker, J.; Vargas, C.; Keller, S. *Anal. Biochem.* **2011**, *418*, 307-309.
34) Velazquez-Campoy, A.; Freire, E. *Nat. Protocols* **2006**, *1*, 186-191.
35) Brandenburg, J. G.; Bannwarth, C.; Hansen, A.; Grimme, S. *J. Chem. Phys.* **2018**, *148*, 064104.
36) Marenich, A. V.; Cramer, C. J.; Truhlar, D. G. *J. Phys. Chem. B* **2009**, *113*, 6378-6396.
37) Adamo, C.; Barone, V. *J. Chem. Phys.* **1999**, *110*, 6158-6170; Weigend, F.; Ahlrichs, R. *PhysChemChemPhys* **2005**, *7*, 3297-3305; Grimme, S.; Ehrlich, S.; Goerigk, L. *J. Comput. Chem.* **2011**, *32*, 1456-1465.
38) Neese, F. *WIREs Comput. Mol. Sci* **2012**, *2*, 73-78.
39) Case, D. A.; Babin, V.; Berryman, J. T.; Betz, R. M.; Cai, Q.; Cerutti, D. S.; Cheatham III, T. E.; Darden, T. A.; Duke, R. E.; Gohlke, H.; Goetz, A. W.; Gusarov, S.; Homeyer, N.; Janowski, P.; Kaus, J.; Kolossváry, I.; Kovalenko, A.; Lee, T. S.; LeGrand, S.; Luchko, T.; Luo, R.; Madej, B.; Merz, K. M.; Paesani, F.; Roe, D. R.; Roitberg, A.; Sagui, C.; Salomon-Ferrer, R.; Seabra, G.; Simmerling, C. L.; Smith, W.; Swails, J.; Walker, R. C.; Wang, J.; Wolf, R. M.; Wu, X.; Kollman, P. A.; University of California: 2016.
40) Wang, J. M.; Wolf, R. M.; Caldwell, J. W.; Kollman, P. A.; Case, D. A. *J. Comput. Chem.* **2004**, *25*, 1157-1174.